Negative effect of cations out-diffusion and auto-doping on switching mechanisms of transparent memristor devices employing ZnO/ITO heterostructure

Firman Mangasa Simanjuntak,[1,2] Sridhar Chandrasekaran,[3] Debashis Panda,[4] Sailesh Rajasekaran,[5] Cut Rullyani,[5] Govindasamy Madhaiyan,[6] Themistoklis Prodromakis,[1,*] and Tseung-Yuen Tseng[2,*]

[1]Centre for Electronics Frontiers, University of Southampton, Southampton SO17 1BJ, U.K.
[2]Institute of Electronics, National Chiao Tung University, Hsinchu 30010, Taiwan
[3]Advanced Research Institute, Dr. MGR Educational and Research Institute, Chennai 600095, India
[4]Department of Physics, National Institute of Science and Technology, Berhampur 761 008, India
[5]Department of Materials Science and Engineering, National Yang Ming Chiao Tung University, Hsinchu 30010, Taiwan
[6]Institute of Physics, National Yang Ming Chiao Tung University, Hsinchu 30010, Taiwan
*Corresponding author: t.prodromakis@soton.ac.uk, tseng@nctu.edu.tw

An excessive unintentional out-diffuses In atoms into the switching layer is a potential threat to the switching stability of memristor devices having indium tin oxide (ITO) as the electrode. We suggest that the physical factor (bombardment of Ar ions and bombardment induced localized heat during ZnO deposition) and chemical factor (bonding dissociation energy, point defects, and bond length of atoms) responsible for promoting the out-diffusion. The In atom acts as dopant in the ZnO lattice that degenerates the ZnO insulative behavior. Furthermore, the In ions take part in the conduction mechanism where they may compete with other mobile species to form and rupture the filament, and hence, deteriorate the switching performance. We propose a facile UV/O_3 (UVO) treatment to mitigate such damaging effects. The device fabricated on the UVO-treated ITO substrate exhibits significant switching parameter improvement than that of the device manufactured on untreated ITO. This work delivers an insight into the damaging effect of out-diffusion and auto-doping processes on the reliability of memristor devices.

Keywords: memristor, resistive memory, surface treatment, ultraviolet/ozone, transparent electronics.

Memristor technology shows promising potential for future universal ultra-high density data storage applications.[1] The realization of high-performance memristor switching devices having transparent architecture could add commercial value for making invisible electronic gadgets[2,3] and has a great potential to be integrated on optoelectronics for wearable applications such as cogni-retina,[4] smart display,[5] artificial skin,[6] synapses,[7,8] etc. The switching mechanism of the memristor relies on the reduction-oxidation process of mobile defect species inside the switching layer to form and rupture conducting filament that switches the device on and off, respectively.[9] Number of species and their mobility and drift path involved during the switching process determines the characteristics of the filament, which influence the switching parameter and stability of the device.

ZnO material has been investigated for more than a decade for the future transparent non-volatile memory; nevertheless, fabricating reliable ZnO-based memristor devices is still a major challenge. Huge efforts have been placed to control the size and shape of the filament to enhance the device stability; several of the proposed techniques include unconventional electroform programming,[10] adding dopant,[11] modulating the deposition parameter,[12–14] employing plasma and chemical treatments,[15,16] and electrode engineering.[17] Yet, these techniques are complicated, time-consuming, and require careful preparation and precise parameters to ensure their efficacy.

Indium tin oxide (ITO) is widely used as a transparent conducting oxide electrode in optoelectronic circuits.[18] UV/O_3 treatment (UVO) on ITO coated substrate becomes one of the mandatory processes to enhance the performance of the organic optoelectronics, and its effect on the ITO material has been extensively investigated.[18–21] On the other hand, characterization of inorganic (metal-oxide) material grown on the ITO substrate to know the impact of such UV/O_3 treatment on the switching characteristics of memristor devices is still less explored.[22,23] Several reports on memristor devices that employ ITO materials suggest that indium (In) and

tin (Sn) atoms originated from the ITO electrode may benefit the switching mechanism in memristor devices.[24–30] However, in our study, we found that an excessive out-diffusion species from the ITO electrode leads to unstable switching; moreover, in contrast to some of those reports, Sn is found to be immobile that may not have a significant role in the switching mechanism.

Commercial ITO coated polyethylene naphthalate (PEN) substrates were ultrasonicated in ethanol, IPA, and DI water for 15 min., sequentially, dried with an N_2 gas gun. Some of the substrates were then surface-treated using UV/O_3 (Jelight 42 OVO cleaner) for 60 min. The O_2 flow rate of UVO treatment was 500 cm^3/min and a low-pressure mercury (Hg) vapor lamp type with an intensity of 28 mW/cm^2 generated wavelength of 185 and 254 nm. The treatment was conducted without additional heating, nevertheless, the temperature inside the chamber may increase due to the irradiation. Hereafter, 50 nm thick ZnO films were deposited onto the substrates using a radio frequency (R.F.) magnetron sputtering employing 50 Watt deposition power in mixed Ar/O_2 ambient (20 sccm Ar and 10 sccm O_2 with a total working pressure of 20 mTorr) at room temperature. 80 nm thick aluminum-doped zinc oxide (AZO) top electrodes were R.F. sputtered and patterned onto the ZnO films with a metal shadow mask having circular shapes with a diameter of 150 μm. The devices or films fabricated on the ITO substrates without and with UVO treatment were denoted as as-received and as-treated devices, respectively. Crystal structure and the surface topography of the films were investigated using a grazing incidence X-ray diffraction (GIXRD, D1. Bede Plc.) and an atomic force microscopy (AFM, D3100). Defect concentration and element profile distribution were examined using an X-ray photoelectron spectroscopy (XPS, PHI Quantera SXM). Electrical characteristics of the devices were measured using a semiconductor device analyzer (B1500SA, Agilent Technologies Inc.). The transparency of the devices was measured using an ultraviolet-visible spectrophotometer (U-3010, Hitachi).

The devices achieve 90% transmittance at a wavelength of 550 nm and an average transmittance of 84% in the visible light spectrum, as depicted in Fig. 1(a). Note that the transmittance of as-received and as-treated devices is identical. This shows that the AZO/ZnO/ITO/PEN stack structure has promising potential for invisible electronics and integration in photonics systems. Figures 1(b) and (c) exhibit the typical I-V curves of the as-received and as-treated devices, respectively. The electrical characteristics were conducted by sweeping a voltage bias at the AZO top electrode while the ITO bottom electrode was ground (inset of Fig. 1(b)); a current compliance (CC) was employed during the negative sweep to avoid permanent breakdown. The devices require a forming process to activate the switching behavior and, thereafter, exhibit clockwise switching characteristics. A -4.3 V sweep with a current compliance of 5 mA was required to switch the as-received device from the pristine state to a low resistance state (LRS, On). Hereafter, the device can be switched to a high resistance state (HRS, Off) employing a positive bias voltage sweep (2.5 V), called as reset; conversely, a negative bias of approximately -2.2 V switches the device back to the LRS, called as set. On the other hand, the as-treated device can be operated at a lower CC (1 mA), and the forming voltage slightly increases to -4.7 V. The device can reset and set with a bias voltage of 2.3 and -1.6 V, respectively. The as-received device exhibits poor endurance; it only has an On/Off ratio of 5 times and the HRS decays after 75 cycles (Fig. 1(d)). Meanwhile, the as-treated devices perform excellent cycle-to-cycle test having an On/Off ratio of more than one order of magnitude with no observable intermediate state (data error) or state decay for more than 1500 cycles (Fig. 1(e)); The as-treated device also exhibits sufficient retention performance,[31–33] see supplementary Fig. S1. Furthermore, it exhibits more satisfactory performance employing such low CC compared to other ZnO-based transparent memristor technologies.[13] This result shows that the UVO surface treatment induced significant

enhancement in device performance. Materials characterization was conducted to elucidate this phenomenon.

The microstructure of ZnO films may influence the switching characteristics of the memristor devices;[12,13] henceforth, we investigated the crystal structure, and the surface topography of the ZnO films grown on the ITO substrate and the results are depicted in Figs. 2(a) and (b), respectively. Both of the ZnO films grown on as-received and as-treated ITO substrates have wurtzite crystal structure with a (002)-preferred orientation.[14] The (002) peak position of as-treated, however, is found to have a higher 2θ angle than that of as-received (inset of Fig. 2(a)). The surface topography of the ZnO grown on the as-treated substrate tends to have a larger grain size and lower surface roughness than the ZnO grown on the as-received substrate (Figs. 2(b)(i) and (ii)). Nevertheless, these results indicate that the UVO treatment does not significantly alter the microstructure properties of the ZnO films, and we infer that such slight microstructure deviation between the two samples has a minor role in determining the performance differences between the as-received and as-treated devices. The chemical properties of the two ZnO films, however, are quite different. We investigate the chemical composition variation across the ZnO films, as depicted in Fig. 2(c). We find a considerable amount of indium species existed in the ZnO film grown on the as-received substrate. Meanwhile, the Indium out-diffusion is limited in the as-treated device. We further conduct a detailed analysis of the out-diffusion phenomenon by evaluating the chemical species in the three different regions across the ZnO films (top (near the surface), middle, and bottom (near the substrate) regions), and the results are shown in Figs. 3(a-d). The $In3d^{5/2}$ core level spectra of all-region are located at approximately 444.8 eV, and their binding energy difference with the $In3d^{3/2}$ is approximately 7.6 eV indicating an oxidation state of 3+; this suggests that the indium species behave as dopant which substituting the Zn atoms in the ZnO matrix.[34,35] Note that there is no significant trace of Sn element in the ZnO films (insets of Figs. 3(a) and (b)).

Such result shows that the indium diffuses out of the ITO substrate and forms In-O bonds in the ZnO lattice. The formation of In-O bonds should affect the concentration of oxygen-related species in the ZnO films.[36] Hence, the O1s spectra are investigated to evaluate the oxygen-related species and are deconvoluted into three Gaussian peaks (Figs. 3(c) and (d)); oxygen concentration in the fully-oxidized lattice (O_I) and oxygen-deficient (O_{II}) regions, and absorbed oxygens (O_{III})).[34] The oxygen vacancy concentration (Vo) is calculated by taking the area ratio of O_{II} and O_I+O_{II},[34] and the result is shown in Fig. 3(e). It is found that the Vo concentration decreases in the deeper region of the films where the as-received sample has a lower Vo concentration in all-region as compared to the as-treated device; this is due to the higher indium concentration in the respective regions and films (Fig. 2(c)). The XPS analysis corroborates with the phenomenon found in the In-doped ZnO system.[35] This evidence shows that the out-diffusion process is also followed by auto-doping mechanism[37] and, thus, it explains why the microstructural alteration occurs in the films. It is reported that the 2θ of (002)-crystal orientation tends to shift to a lower angle in the ZnO film having higher In concentration[38] (as-received, Fig. 2(a)) due to the substitution of Zn^{2+} ions (radius 88 pm) with the large In^{3+} ions (radius 94 pm) and, consequently, it prevents the grain growth and may slightly increase the roughness of the films (Fig. 2(b)(i)).[35,38] We suggest that the indium out-diffusion arises from the physical and chemical processes involved during the sputtering deposition. The schematic of the diffusion mechanism in as-received and as-treated samples is shown in Figures 3(f)(i) and (ii), respectively. It is reported that the mean-free-path of the sputtered species (originated from the sputter target) is significantly shorter than the substrate-to-target distance indicating that most of these species are collided with Ar ions across the Debye sheath before reaching the substrate.[39] This collision, eventually, makes the high energetic Ar ions bombard the surface of the substrate and the growing film.[39] The Ar ions bombardment build up local transient surface heating, and adatom induces resputtering mechanisms that responsible for “ejecting” some

atoms from beneath the surface of the substrate to the surface and diffuse to interface and grown film (Fig. 3(f)(i)).[40] These mechanisms can be found to be more serious when depositing materials onto semiconductor substrates,[41] especially ITO substrate that has a rough surface condition.[23] Based on the XPS analysis (Figs. 2(c) and 3(a-b)), indium is the only out-diffused species; this is due to several reasons include: (i) In is the main element in the ITO system while the Sn, as a dopant, is usually added with a much lower concentration;[19] (ii) Sn-O has higher bonding dissociation energy (548 kJ/mol) than that of In-O (360 kJ/mol)[42] which make it easier for the Ar ions or bombardment induced localized heat to break the In-O bonds; (iii) In-O may have lower surface energy than that of ZnO at the ZnO/ITO interface.[43] Once the indium has diffused to the surface of the ITO, the indium can easily diffuse across the ZnO layer. Several factors that can lower the energy barrier for this diffusion include: (i) the bond length of Zn-O, Zn-Zn, and O-O is approximately 200, 324, and 260 pm, respectively, which is much greater than the ionic radius of In^{3+};[44–46] (ii) ZnO has many dangling bonds and vacancies defects providing diffusion paths for the indium to diffuse within the lattices;[43,46,47] (iii) indium is found to have a high diffusion coefficient in ZnO.[48] The diffusion rate of the indium is hindered after the UVO treatment, and the diffusion rate is found to decrease as the treatment time increases (see supplementary Figure S2). We suggest this is due to the fact that the UVO induces the formation of an oxygen-rich thin layer at the surface of the ITO, providing a significant decrease in the total ratio of indium concentration and reducing the number of dangling bonds.[18,19] Consequently, this thin layer will limit the number of indium that can be “ejected” onto the surface (Fig. 3(f)(ii)); the concentration of the out-diffused indium in the as-treated device is almost similar across the ZnO layer, indicating a low diffusion rate of indium (Figs. 2(c) and 3(b)).

Based on the above material analysis, we propose the conduction mechanism to explain the electrical phenomenon in the devices, as shown in Fig. 4. Based on our electrical analysis,

the conduction of electron in our devices follows the typical filamentary mechanism (see supplementary Figs. S3 and S4).[31,49,50] The as-received pristine device has a high amount of In and act as an electron donor dopant[38,48] and, thus, the pristine device has high leakage current and require a CC as low as 5 mA to electroform the device (Fig. 1(b)); see supplementary Fig. S5 for the schematic of the band diagram in the supplementary material. Since In^{3+} has high mobility in metal oxides,[47,48] we suggest the In^{3+} will also take part in the formation of the filament along with oxygen vacancy defects that grow from the top AZO/ZnO interface with the apex at the ZnO/ITO bottom interface (Fig. 4(a)(i) and (ii)). During the reset process, the positive bias repulses the oxygens that accumulate at the bottom interface to recombine with the oxygen vacancy in the filament, meanwhile, the In atoms in the filament are re-ionized and attracted to the bottom electrode; hence, this process ruptures the conducting filament (Figs. 4(a)(iii) and (iv)). Similarly, the set process occurs in the reverse fashion where the negative bias re-ionize the oxygens to create oxygen vacancies while the In ions are repulsed toward the top interface and rejuvenate the conducting filament (Figs. 4(a)(i) and (v)). Oxygen and indium atoms are competing to contribute in rupturing and rejuvenating the filament, of which they drift in the opposite direction under an electric field. This competition may affect the stability of the device. Moreover, it is reported that cation may be reduced in the midway before reaching the filament or interface during the set and reset processes, respectively.[51] Hence, there is also a possibility the In ions are reduced or react with the oxygens forming In or In-O clusters, respectively, in the midway (the gap between the remnant conducting filament and oxide/electrode interface) by considering the fact that the cation mobility (In^{3+}) is higher than anion (O^{2-}).[52] Therefore, this repeated competition during the set and reset processes may result in the difficulty for the device to rupture the filament (HRS decay) and affect the performance instability after subsequent switching (Fig. 1(d)). On the other hand, the as-treated device only has a small trace of indium in the switching layer (Fig. 4(b)(i)) and exhibits a lower pristine

leakage current than that of the as-received device (Fig. 1(c)); thus, the electroforming process can be conducted employing a lower CC (1 mA). We can assume that the size of the filament in the as-treated device is smaller than that in the as-received device due to the employment of small CC and minor contribution of In ions in the formation of the filament (Fig. 4(b)(ii)). Note that the as-treated device requires a slightly higher forming voltage than that in the as-received device; this is due to the fact that the UVO enhances the work function of the ITO, resulting in a higher barrier at the ZnO/ITO interface (see supplementary Table S1).[19] The UVO treatment also provide abundant oxygens on the surface of the ITO, which beneficial in creating a larger gap during the reset process and, consequently, results in a higher On/Off ratio than that of the as-received device (Figs. 4(b)(iii) and (iv), Fig. 1(e)). We suggest that the contribution of out-diffused indium atoms during the set and reset processes should be minimized to avoid reduction-oxidation competition between mobile species during the switching process in order to achieve a highly stable device as performed by the as-treated device (Fig. 4(b)(iii) and (v), Fig. 1(e)).

In conclusion, we investigated the damaging effect of indium out-diffusion on the switching performance of the ZnO-based transparent memristor device. The indium originated from the ITO substrate diffuses into the switching layer induced by physical and chemical processes during the ZnO deposition onto the ITO substrate. The out-diffused indium atoms act as dopants to donor electrons in ZnO lattices, and the atoms are also involved in the switching process and degenerating the stability of the device. The employment of a facile conventional UV/O_3 treatment on the ITO substrate promotes the formation of an oxygen-rich thin layer on the surface of the ITO that inhibits the diffusion of the In atoms into the ZnO. Henceforth, the competition between mobile species (indium cations and oxygen anions) to rejuvenate and rupture the filament during the set and reset processes, respectively, can be minimized and improve the stability of the device. Beside UVO treatment, we hypothesis that peroxide and O_2

plasma treatments on ITO substrate as well as optimizing the ZnO deposition parameter (such as the employment of low sputtering power, a short distance between the target to the substrate, and increasing mean-free-path of sputtered species) could also help to hinder the indium out-diffusion; these techniques will be explored in our future studies. This study elucidates the role of cation out-diffusion and auto-doping phenomenon in the switching mechanism, which is crucial to be taken into account in fabricating high-performance transparent memristor devices and offer a simple method to mitigate the damaging effect and prolong the device operation.

Supplementary Material

Supplementary material contains additional data on Indium profile across the AZO/ZnO/ITO stack, curve fitting analysis, barrier height calculation, and the schematic of band diagram.

Acknowledgment

The Ministry of Science and Technology, Taiwan, supported by this work under project MOST 105-2221-E-009-134-MY3 and NCTU visiting research fellowship program. F. M. Simanjuntak and T. Prodromakis acknowledge the support of EPSRC Programme Grant (EP/R024642/1) and H2020-FETPROACT-2018-01 SYNCH project. D. Panda acknowledged the DST-SERB research grant, Govt. of India (Grant no: SRG/2019/000129) to support this work. The authors thank Eric Chu (Jelight Co. Inc.) for providing the detail information on the UVO equipment.

Data availability

The data that support the findings of this work are available from the corresponding author upon reasonable request.

References

[1] S. Salahuddin, K. Ni, and S. Datta, Nat. Electron. **1**, 442 (2018).

[2] G. Thomas, Nature **389**, 907 (1997).

[3] J.F. Wager, Science (80-.). **300**, 1245 (2003).

[4] D. Berco and D. Shenp Ang, Adv. Intell. Syst. **1**, 1900012 (2019).

[5] P.-K.K. Yang, C.-H.H. Ho, D.-H.H. Lien, J.R. Durán Retamal, C.-F.F. Kang, K.-M.M. Chen, T.-H.H. Huang, Y.-C.C. Yu, C.-I.I. Wu, and J.-H.H. He, Sci. Rep. **5**, 1 (2015).

[6] C. Zhang, W. Bin Ye, K. Zhou, H. Chen, J. Yang, G. Ding, X. Chen, Y. Zhou, L. Zhou, F. Li, and S. Han, Adv. Funct. Mater. **29**, 1808783 (2019).

[7] F. Gul, Appl. Nanosci. **10**, 611 (2020).

[8] S.H. Jo, T. Chang, I. Ebong, B.B. Bhadviya, P. Mazumder, and W. Lu, Nano Lett. **10**, 1297 (2010).

[9] J.J. Yang, M.D. Pickett, X. Li, D.A.A. a Ohlberg, D.R. Stewart, and R.S. Williams, Nat. Nanotechnol. **3**, 429 (2008).

[10] F.M. Simanjuntak, D. Panda, T.-L. Tsai, C.-A. Lin, K.-H. Wei, and T.-Y. Tseng, Appl. Phys. Lett. **107**, 033505 (2015).

[11] F.M. Simanjuntak, O.K. Prasad, D. Panda, C.-A. Lin, T.-L. Tsai, K.-H. Wei, and T.-Y. Tseng, Appl. Phys. Lett. **108**, 183506 (2016).

[12] F.M. Simanjuntak, T. Ohno, and S. Samukawa, ACS Appl. Electron. Mater. **1**, 2184 (2019).

[13] F.M. Simanjuntak, T. Ohno, and S. Samukawa, AIP Adv. **9**, 105216 (2019).

[14] F. Gul and H. Efeoglu, Superlattices Microstruct. **101**, 172 (2017).

[15] F.M. Simanjuntak, T. Ohno, S. Chandrasekaran, T.-Y. Tseng, and S. Samukawa, Nanotechnology **31**, 26LT01 (2020).

[16] F.M. Simanjuntak, S. Chandrasekaran, C. Lin, and T.-Y. Tseng, APL Mater. **7**, 051108 (2019).

[17] F.M. Simanjuntak, D. Panda, T.-L. Tsai, C.-A. Lin, K.-H. Wei, and T.-Y. Tseng, J. Mater. Sci. **50**, 6961 (2015).

[18] S.Y. Kim, J. Appl. Phys. **95**, 2560 (2004).

[19] P. Destruel, H. Bock, I. Séguy, P. Jolinat, M. Oukachmih, and E. Bedel-Pereira, Polym. Int. **55**, 601 (2006).

[20] M.F. Lo, T.W. Ng, H.W. Mo, and C.S. Lee, Adv. Funct. Mater. **23**, 1718 (2013).

[21] T. Hu, F. Zhang, Z. Xu, S. Zhao, X. Yue, and G. Yuan, Synth. Met. **159**, 754 (2009).

[22] X. Teng, H. Fan, S. Pan, C. Ye, and G. Li, Mater. Lett. **61**, 201 (2007).

[23] K. Cang, L.Y. Liang, Z.M. Liu, L. Wu, H. Luo, H.T. Cao, and Y.S. Zou, J. Alloys Compd. **550**, 258 (2013).

[24] B. Sun, X. Han, R. Xu, and K. Qian, ACS Appl. Electron. Mater. **2**, 1603 (2020).

[25] P.J. Yang, S. Jou, and C.C. Chiu, Jpn. J. Appl. Phys. **53**, (2014).

[26] X. Wu, H. Xu, Y. Wang, A.L. Rogach, Y. Shen, and N. Zhao, Semicond. Sci. Technol. **30**, 074002 (2015).

[27] Z.H. Lin and Y.H. Wang, Appl. Phys. Lett. **109**, 0 (2016).

[28] K. Qian, R.Y. Tay, M.F. Lin, J. Chen, H. Li, J. Lin, J. Wang, G. Cai, V.C. Nguyen, E.H.T. Teo, T. Chen, and P.S. Lee, ACS Nano (2017).

[29] C. Ye, T.F. Deng, J. Wu, C. Zhan, H. Wang, and J. Zhang, Jpn. J. Appl. Phys. **54**, 0 (2015).

[30] S. Rajasekaran, F.M. Simanjuntak, D. Panda, S. Chandrasekaran, R. Aluguri, A. Saleem, and T.-Y. Tseng, ACS Appl. Electron. Mater. **2**, 3131 (2020).

[31] E. Lim and R. Ismail, Electronics **4**, 586 (2015).

[32] A. Sawa, Mater. Today **11**, 28 (2008).

[33] A. Yesil, F. Gül, and Y. Babacan, in *Memristor and Memristive Neural Networks* (InTech, 2018).

[34] H.J. Kim, J. Jung, and H.J. Kim, Sci. Rep. **10**, 1 (2020).

[35] S. Chirakkara, K.K. Nanda, and S.B. Krupanidhi, Thin Solid Films **519**, 3647 (2011).

[36] A. Singh, S. Chaudhary, and D.K. Pandya, Acta Mater. **111**, 1 (2016).

[37] W.H. Shepherd, J. Electrochem. Soc. **115**, 652 (1968).

[38] D.H. Kim, N.G. Cho, H.G. Kim, and W.-Y. Choi, J. Electrochem. Soc. **154**, H939 (2007).

[39] K.-C.C. Liu, W.-H.H. Tzeng, K.-M.M. Chang, and C.-H.H. Wu, Surf. Coatings Technol. **205**, S379 (2010).

[40] X.W. Zhou and H.N.G. Wadley, Surf. Sci. **431**, 58 (1999).

[41] D.W. Moon, Y. Ha, H.K. Kim, K.J. Kim, H.S. Kim, J.Y. Lee, and S. Kim, Appl. Surf. Sci. **150**, 235 (1999).

[42] J.A. Dean, *Lange's Handbook of Chemistry*, 15th ed. (McGraw-Hill, New York, 1999).

[43] H. Dong, W. Cabrera, R. V. Galatage, K. Santosh, B. Brennan, X. Qin, S. McDonnell, D. Zhernokletov, C.L. Hinkle, K. Cho, Y.J. Chabal, and R.M. Wallace, Appl. Phys. Lett. **103**, 2 (2013).

[44] P. Lommens, P.F. Smet, C. De Mello Donega, A. Meijerink, L. Piraux, S. Michotte, S. Mátéfi-Tempfli, D. Poelman, and Z. Hens, J. Lumin. **118**, 245 (2006).

[45] J. Wu, F. Long, B. Tang, and X. Tang, AIP Adv. **8**, (2018).

[46] A. Janotti and C.G. Van de Walle, Phys. Rev. B **76**, 165202 (2007).

[47] Y. Hu, C. Wang, H. Dong, R.M. Wallace, K. Cho, W.H. Wang, and W.H. Wang, ACS Appl. Mater. Interfaces **8**, 7595 (2016).

[48] T. Nakagawa, K. Matsumoto, I. Sakaguchi, M. Uematsu, H. Haneda, and N. Ohashi, Jpn. J. Appl. Phys. **47**, 7848 (2008).

[49] F. Gül, Results Phys. **12**, 1091 (2019).

[50] F. Gul and H. Efeoglu, Ceram. Int. **43**, 10770 (2017).

[51] Y. Yang, P. Gao, L. Li, X. Pan, S. Tappertzhofen, S. Choi, R. Waser, I. Valov, and W.D. Lu, Nat. Commun. **5**, 4232 (2014).

[52] C.F. Chang, J.Y. Chen, C.W. Huang, C.H. Chiu, T.Y. Lin, P.H. Yeh, and W.W. Wu, Small **13**, 1 (2017).

Figure Captions

Figure 1. (a) ultraviolet-visible light transmittance of the AZO/ZnO/ITO devices. Typical I-V curves of (b) as-received and (c) as-treated devices. Insets in (a) and (b) show the photographs of the fabricated devices and the schematic of electrical measurement setup of the device.

Figure 2. (a) GI-XRD of ZnO films deposited on as-received and as-treated ITO substrates. (b) AFM topography of ZnO films grown on (i) as-received and (ii) as-treated ITO substrates. (c) Atomic concentration profile in AZO/ZnO/ITO films stack calculated from depth-XPS analysis.

Figure 3. In3d core level spectra of ZnO films grown on (a) as-received and (b) as-treated ITO substrates. O1s core level spectra of ZnO films grown on (c) as-received and (d) as-treated ITO substrates. (e) Oxygen vacancies concentration in the ZnO films calculated from (c) and (d). (f) Cations diffusion mechanism in (i) as-received and (ii) as-treated samples. Inset in (a) and (b) show no intensity comes from Sn3d core level spectra in the ZnO films. XPS spectra in (a-d) were taken at three different depth position.

Figure 4. Schematic of the conduction mechanism during forming, reset and set processes in (a) as-received and (b) as-treated devices.

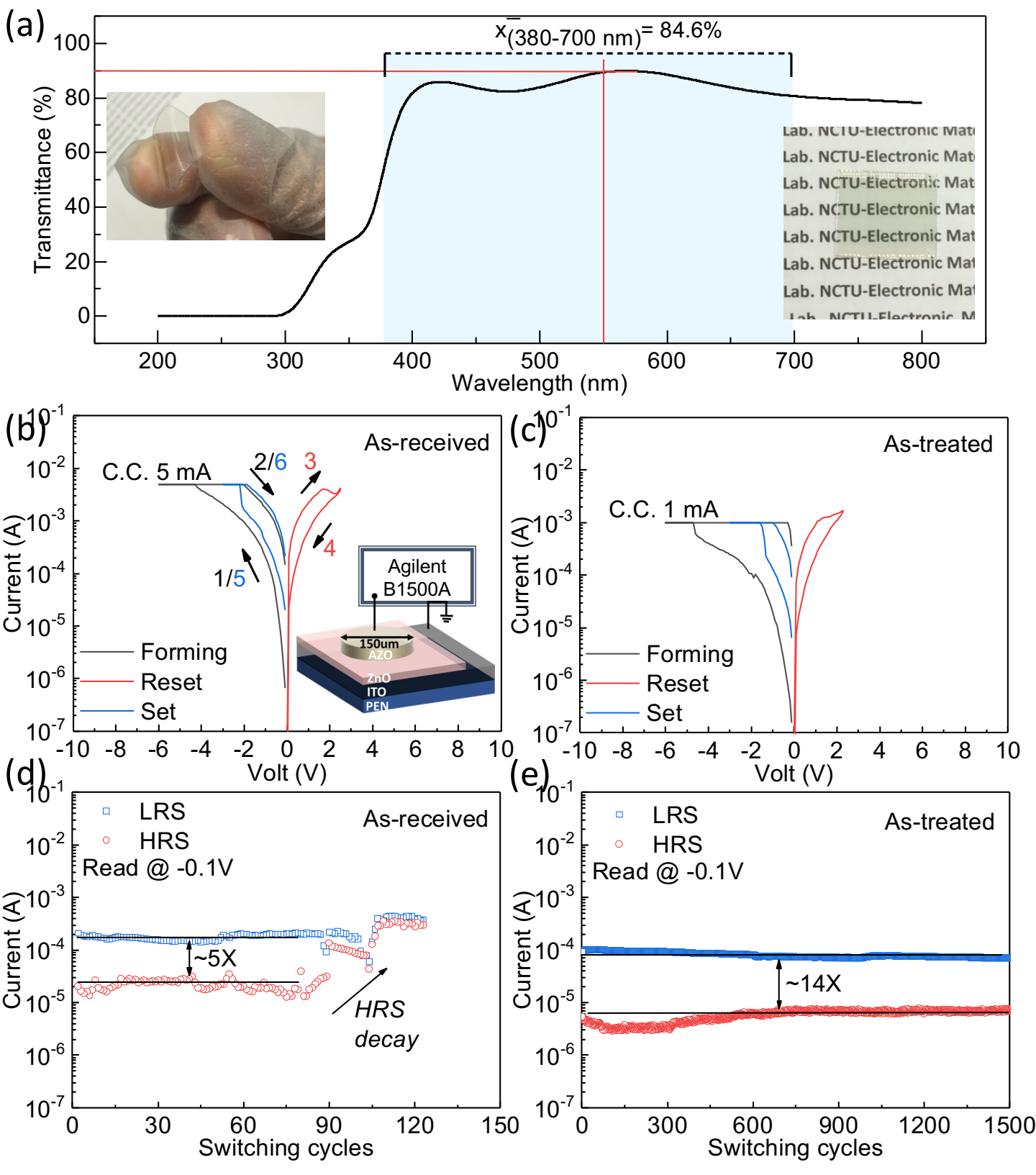

Figure 1 Simanjuntak et al.

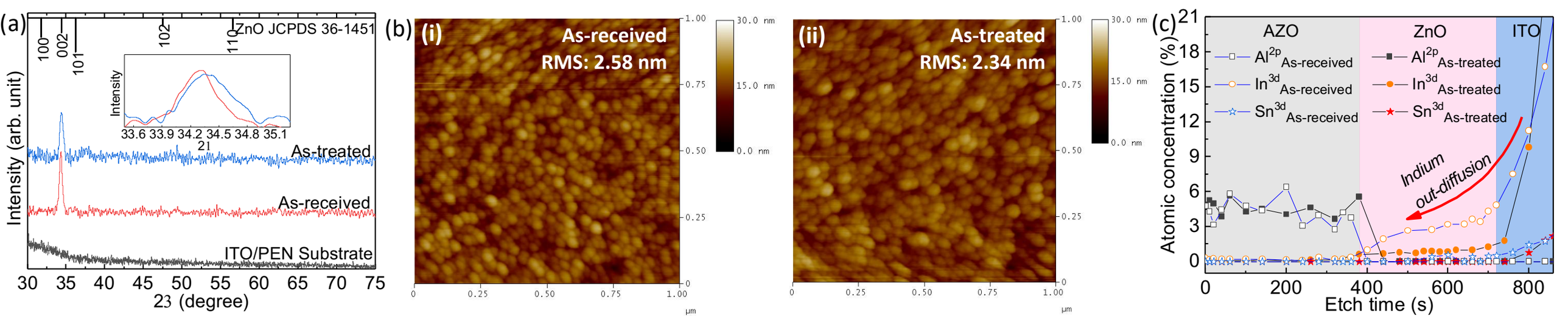

Figure 2 Simanjuntak et al.

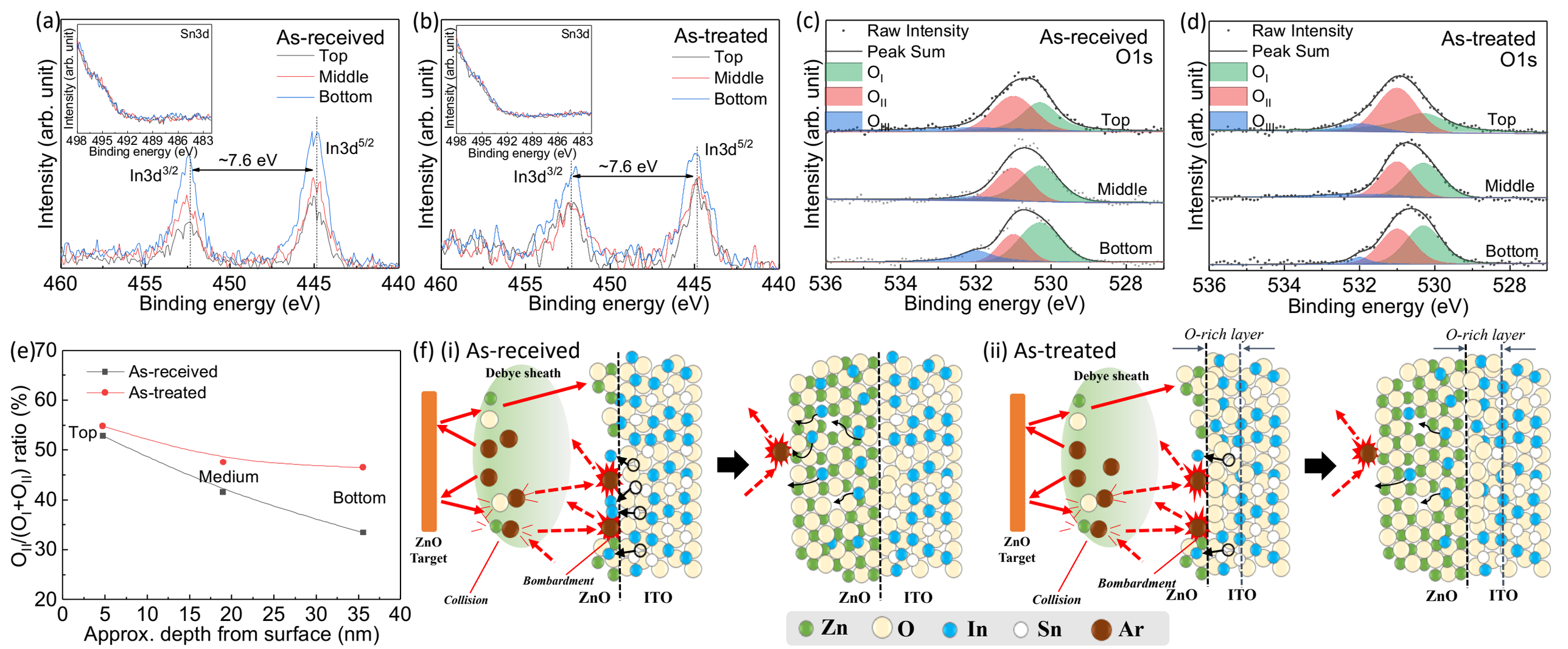

Fig. 3 Simanjuntak et al.

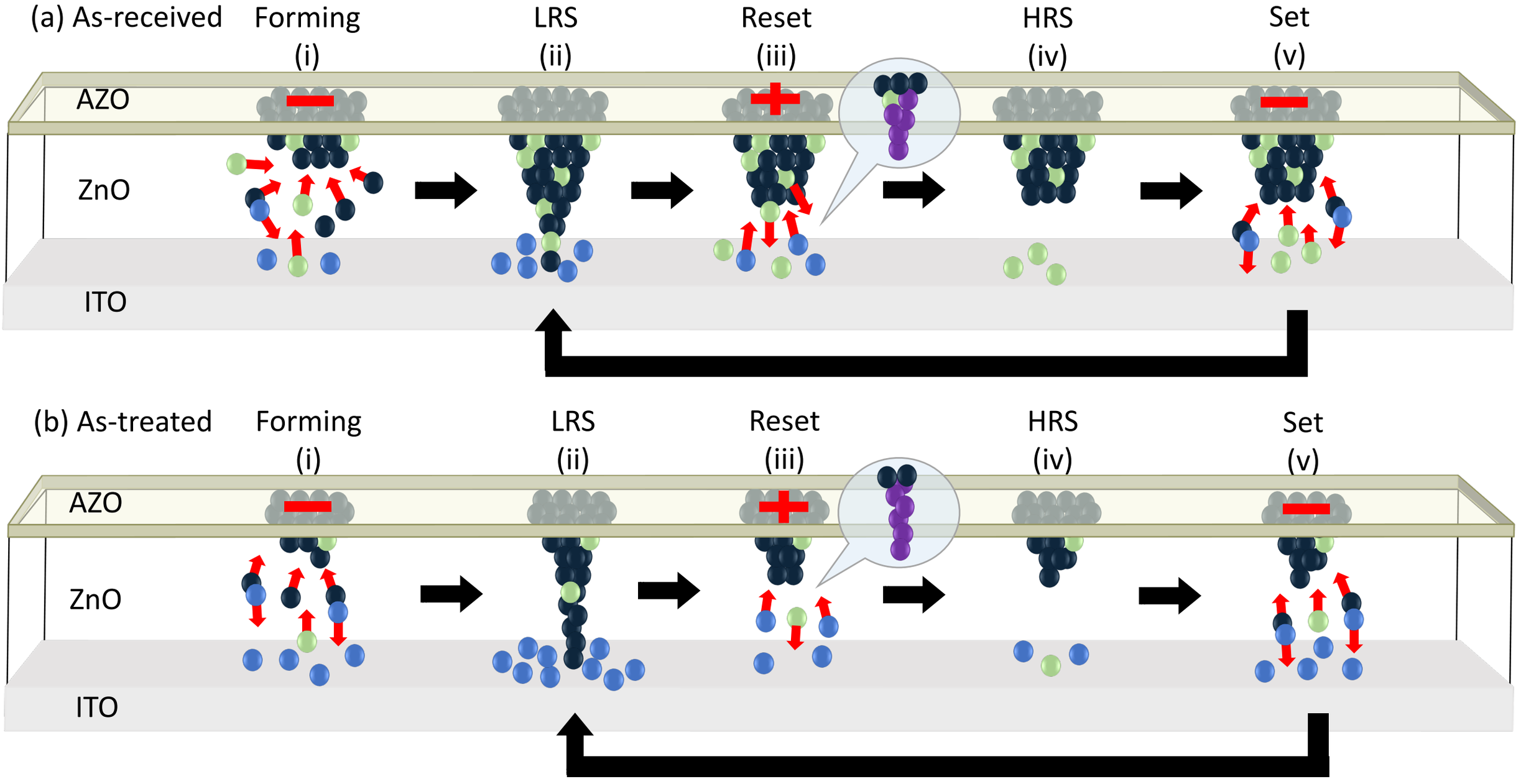

Figure 4 Simanjuntak et al.